Synthesis and Characterization of Nylon-6/Mesoporous Silica Nanocomposites via *In Situ* Synchronous Hydrolytic Polymerization of Tetraethylorthosilicate and ε-Caprolactam

Lanjie Li,[1,2] Guisheng Yang[1,3]

[1]*CAS Key Laboratory of Engineering Plastics, Joint Laboratory of Polymer Science and Materials, Institute of Chemistry, the Chinese Academy of Sciences, Beijing 100080, People's Republic of China*
[2]*Graduate School of the Chinese Academy of Sciences, Beijing 100039, People's Republic of China*
[3]*Shanghai Genius Advanced Materials Co. Ltd, Shanghai 201109, People's Republic of China*

Received 20 September 2009; accepted 26 August 2010
DOI 10.1002/app.33289
Published online 7 December 2010 in Wiley Online Library (wileyonlinelibrary.com).

ABSTRACT: Nylon 6 (N6)/mesoporous silica (MS) nanocomposites (NMSNs) were synthesized via *in situ* synchronous hydrolytic polymerization of tetraethylorthosilicate (TEOS) and ε-caprolactam. The novelty of this technique lies in that the nanosilica generated *in situ* has unique mesoporous structure and ultrahigh-specific surface area (SSA). Mechanical test showed that, compared to conventional precipitated silica (PS) nanofillers, the MS generated *in situ* shows better reinforcing efficiency on N6. At a loading of only 3.0 wt % MS, the tensile modulus, flexural modulus, and the heat distortion temperature of NMSNs exhibit increase of 54.8%, 77.9%, and 55.9°C, respectively. The effects of MS on the crystallization behaviors of N6 have been studied by differential scanning calorimetry (DSC), which shows that the incorporation of MS influences the crystallization behaviors of N6 obviously: (1) increases crystallization temperature (T_c) by serving as heterogonous nucleating agent; (2) favors the formation of γ-phase by hindering the mobility of N6 chains. Dynamic mechanical analysis confirmed that, compared ti that of neat N6, the temperature of the main α-relaxation (T_α) and the secondary β-relaxation (T_β) of NMSNs is shifted 6.1°C and 5.3°C toward higher temperature. © 2010 Wiley Periodicals, Inc. J Appl Polym Sci 120: 1957–1964, 2011

Key words: fillers; mechanical properties; nanocomposites; nylon; silicas

INTRODUCTION

Incorporation of inorganic nanofillers such as clay[1–3] and silica[4,5] into polymer matrix is always attractive because of scientific and engineering points of view. For fabricating high-performance polymer-based nanocomposites, different techniques have been developed, among which sol–gel hybridization and *in situ* polymerization are the two most successful methods.

Inorganic–organic hybrid nanocomposites using sol–gel process where the inorganic phase is grown *in situ* is being actively pursued.[6,7] Sol–gel hybridization centers on the growth of the silica from the hydrolysis-condensation of alkoxysilanes like TEOS in a solution containing the polymer. So far, many polymer/silica nanocomposites have been prepared in this way using poly(vinyl acetate),[8,9] poly(methyl methacrylate),[10] natural rubber,[11] poly(vinyl alcohol),[12] epoxy resin,[13] poly(dimethylsiloxane),[14] acrylic rubber,[15,16] polyimide,[17–19] and polyamide 66.[20]

In situ polymerization, where monomers polymerize into polymer in the presence of nanofillers, is another effective technique. This technique is extraordinarily effective to prepare nylon 6 (N6)-based nanocomposites via hydrolytic ring-opening polymerization of ε-caprolactam, because ε-caprolactam and water can serve as excellent dispersing agents for nanofillers. Many nanocomposites based on N6 have been fabricated by adding nanoparticles, such as carbon nanotubes,[21] montmorillonite,[22] and silica,[23] into the hydrolytic polymerization system of ε-caprolactam.

In this work, we prepared N6/mesoporous silica (MS) nanocomposites (NMSNs) via a method combining the advantages of sol–gel hybridization and *in situ* polymerization. The novelty of this work lies in the fact that both silica and N6 have been grown *in situ* synchronously via hydrolytic polymerization mechanism. By this method, the silica nanoparticles generated *in situ* not only uniformly dispersed in polymer phase, but also have mesoporous structure and ultrahigh-specific surface area (SSA). Compared

Correspondence to: G. Yang (ygs@geniuscn.com).

TABLE I
Formulation, Composition, and Sample Codes of the Prepared Samples

Sample code	ε-Caprolactam (g)	TEOS (g)	Adipic acid (g)	Precipitated silica (g)	Silica content (wt %)	
					Theoretical[a]	Experimental[b]
N6	2000	0.0	10.00	–	0.00	0.0
NMSN05	1990	36.80	9.95	–	0.50	0.49
NMSN15	1970	110.0	9.85	–	1.50	1.53
NMSN30	1940	220.0	9.70	–	3.00	3.04
NPSN30	1940	–	9.70	60	3.00	3.07

[a] The weight percent SiO_2 was calculated assuming full condensation of TEOS and ε-caprolactam.
[b] Residue from gravimetric analysis carried out in a muffle furnace in air at 800°C.

to traditional precipitated silica (PS), this kind of MS shows better reinforcing efficiency on N6.

EXPERIMENTAL

Materials

Commercial grade ε-caprolactam was obtained from Nanjing Oriental Chemical Company. Analytical grade tetraethylorthosilicate (TEOS), adipic acid, formic acid, and ethanol were bought from National Reagent Group Co., China. PS (Ultrasil VN3, size range = 20–100 nm) was bought from Bayer, India.

Preparation of NMSNS and N6

Nylon-6/MS nanocomposites were prepared following the two steps below:

1. A desired amount of TEOS was dissolved in two times of water containing 20-mL formic acid, mixed, and heated to 60°C for 8 h to finish hydrolysis reaction of TEOS. ε-Caprolactam (2000 g) and 200-mL deionized water were then added and mixed. Afterward, the ethanol and formic acid were removed by vacuum distillation.
2. After adding 10 g of adipic acid, the system was heated to 250–260°C under a nitrogen atmosphere in a steel reactor equipped with nitrogen inlet and mechanical mixer. Simultaneously, the pressure was increased to 2.0–2.4 MPa. Afterward, it was maintained for 3 h to achieve prepolymerization of ε-caprolactam and silicic acid in the presence of water. The pressure then began to level off by discharging water vapor slowly, and the reaction was further carried out at atmospheric pressure for 1 h. Finally, postpolymerization was performed at 200–300 Pa until the system viscosity stop increasing. Nylon-6/MS nanocomposites were then obtained and denoted as NMSN.

For purpose of comparison, neat nylon-6 was prepared following step (2) and denoted as N6. Conventional N6/silica nanocomposite was also prepared in the same manner by adding PS and designated as NPSN. The loading of PS was kept at 3.0 wt % of composite, solely for comparative purpose.

Finally, all samples were extracted with boiling water for 48 h and then dried under vacuum at 100°C for 48 h. The formulation, composition, and sample code of the prepared samples are listed in Table I.

Characterization

Transmission electronic microscopy (TEM), scanning electronic microscopy (SEM), and atomic force microscopy (AFM) were used to observe the dispersion and morphology of MS in NMSN.

SEM was performed in a JEOL 6400 microscopy at an acceleration voltage of 10 kV. The fracture surface was coated with 20 nm of gold in a Palaron sputtering apparatus before observation.

TEM was carried out on a JEOL-2100F microscopy at an acceleration voltage of 100 kV. The NMSN sample was ultramicrotomed with a diamond knife on a Leica Ultracut UCT at −20°C to get an 80-nm ultrathin section. To observe the mesoporous structure of silica directly, the N6 phase in NMSNs was completely burned out by calcinations of NMSN30 at 700°C for 8 h. The obtained silica powder was dispersed in ethanol, and a drop of the dispersion was dripped on a copper grid. To observe the semi-interpenetrating network between N6 and silica, the samples for TEM were prepared as follows: 0.1 g of NMSN30 was dissolved in 10 mL trifluoroethanol (TFE), and then the silica nanoparticles were precipitated by centrifugation to wash away the N6 enwrapping the silica nanoparticles; the obtained precipitate was dissolved in 10 mL TFE to form diluted dispersion, and then a drop of the dispersion was dripped on a copper grid.

Tapping mode AFM images were obtained with a VeecoDigital Instruments scanning probe microscopy with Nanoscope IIIa with tapping mode

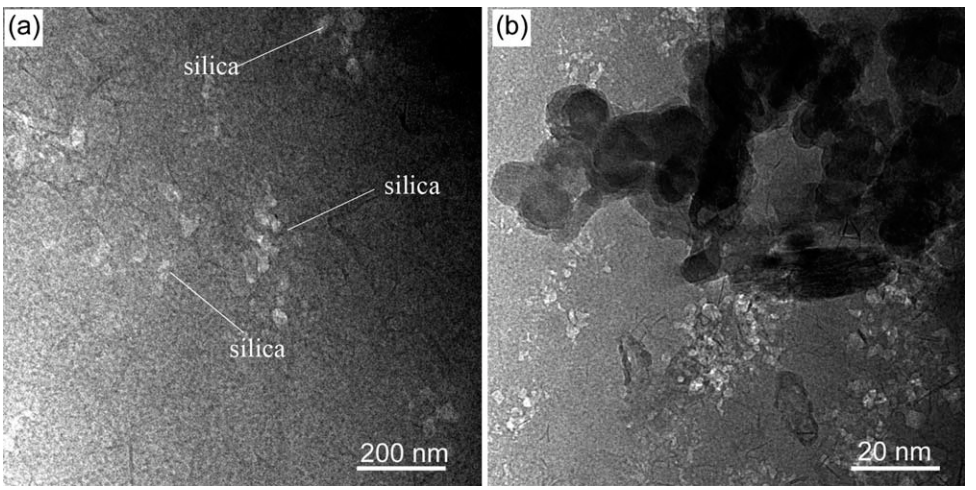

Figure 1 TEM images of NMSN30 at different magnifications.

(Model RTESP) probes for morphological investigation. Ultrathin section of NMSN30 with 200-nm thickness was used for AFM imaging.

BET measurement (TriStar 3000, Micromeritics) was used to measure the surface area, total pore volume, and average pore diameter of the MS powder obtained by burning NMSN30 at 700°C in a muffle furnace for 8 h to remove the polymer phase. Before measurement, all the samples were outgassed at 110°C for 4 h. The measurement was carried out by the sorption of nitrogen gas.

For measurements of mechanical properties, the samples were directly injection molded into standard testing specimens according to ASTM. The IZOD notched impact strength was measured according to ASTM D 256, using an IZOD machine Model CSI-1370. The tensile tests were performed on an Instron machine series 1122 according to ASTM D 638 at a crosshead speed of 50 mm min^{-1}. The bending tests were carried out on the same instrument according to ASTM D 790 at a crosshead speed of 5mm/min. Heat distortion tests were carried out according to ASTM D 648-2001.

Dynamic mechanical analysis (DMA) was performed over a temperature range of −125–150°C with a Netzsch DMA 242 at a heating rate of 3°C min^{-1} and a frequency of 1 Hz.

Differential scanning calorimetry (DSC) measurements were carried out on a NETZSCH DSC 200 PC calibrated by in standards. All the measurements were first performed from 50 to 250°C at a heating rate of 10°C min^{-1} under nitrogen atmosphere, and the samples were held at that temperature for 10 min to erase any previous thermal history and then drop from 250 to 50°C and start the second heating scan. The melt enthalpy (ΔH_f), which is a measure of the degree of crystallinity, was used for comparison of the relative changes in the crystallinity of N6 and determined according to the following equation:

$$Xc, (DSC) = \frac{\Delta Hf}{(1-\phi) \times \Delta Hf^*} \times 100\%$$

where ΔH_f is the melting enthalpy of N6 in the samples, Φ is the weight fraction of silica in the NMSs, and ΔH_f^* is the melting enthalpy of the matrix polymer with 100% crystallinity ($\Delta H_f^* = 190$ J g^{-1} [24,25]).

RESULTS AND DISCUSSION

The morphology and dispersion of MS in the N6 matrix

The TEM images of NMSN30 at different magnifications are shown in Figure 1. At low magnification [Fig. 1(a)], the MS in the NMSN is too vague to be clearly observed. The picture of high magnification [Fig. 1(b)] gives a relatively clear image of MS, which shows that the MS particles have irregular shape; however, the observation effect is also unsatisfactory. It is obvious that the image contrast of the MS particles is very low; therefore, TEM cannot give an image that can clearly reflect the morphology and dispersion of MS on the whole (the reason will be discussed later).

The TEM images of NMSN30 are shown in Figure 2. Although the micromorphology of MS cannot be clearly seen due to the resolution limitation of SEM, it can be seen that MS particles (small white dot in Fig. 2) are dispersed uniformly in N6 matrix.

To clearly observe the dispersion of MS in N6 matrix, the AFM phase images for NMSN30 are also given, as shown in Figure 3. It is clearly shown that the MS particles have irregular shape. The size distribution of MS is very uneven, ranging from tens to hundreds nanometers. In spite of the differences in morphology and size, these nanosized silica particles are dispersed uniformly in N6 matrix.

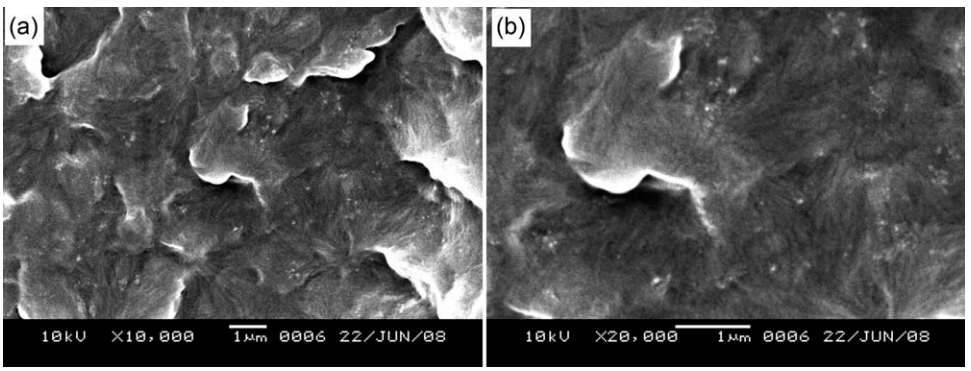

Figure 2 SEM images of NMSN30 at different magnifications.

Figure 4(a) shows the TEM picture of MS particles after the N6 phase was removed by a method previously mentioned. As shown in Figure 4(a), the porous structure of MS can be clearly seen. The pore size is estimated to be about 10 nm. Generally speaking, the pores in the range of 2–50 nm are denoted mesopores[26]; therefore, the silica generated *in situ* in this study is mesoporous filler. Because polymer phase and silica phase are generated synchronously during polymerization, it is reasonable to deduce that N6 phase penetrates in the MS network, consequently, a semi-interpenetrating network forms in every nanosized MS particles. After the N6 enwrapping MS particles was washed away, the obtained silica particles were observed by TEM. As shown in Figure 4(b), a lot of fiberlike N6 phase is found present on the surface. Being strongly immobilized by these mesopores, the N6 phase in mesopores cannot be easily washed away; therefore, when washed by solvent of N6, fiberlike N6 phase can form these MS nanoparticles.

BET measurement of MS

The BET measurement curves of MS are shown in Figure 5, in which Figure 5(a) is the nitrogen sorption and desorption curve from which the SSA can be determined, and Figure 5(b) shows the pore size distribution of MS. The detailed data of BET test are collected in Table II. It is known that mesoporous nanoparticle has much higher SSA than conventional nanoparticle. As shown in Table II, the SSA of MS measured by BET is 632 m^2/g, indicating that the MS generated *in situ* has ultrahigh SSA. The mean pore size of MS is 14.2 nm with a broad size distribution from 2 to 50 nm, as shown in Figure 5(b). The single-point adsorption total pore volume of pores is tested to be 3.21 cm^3/g. For Ultrasil VN3, the PS used as comparison, the SSA is only 132 m^2/g, much lower than that of MS, and no pore is detected.

Ultrahigh SSA means huge contact surface between N6 and silica, and porous structure indicates that some N6 chains are immobilized in these mesopores. According to the pore volume of silica

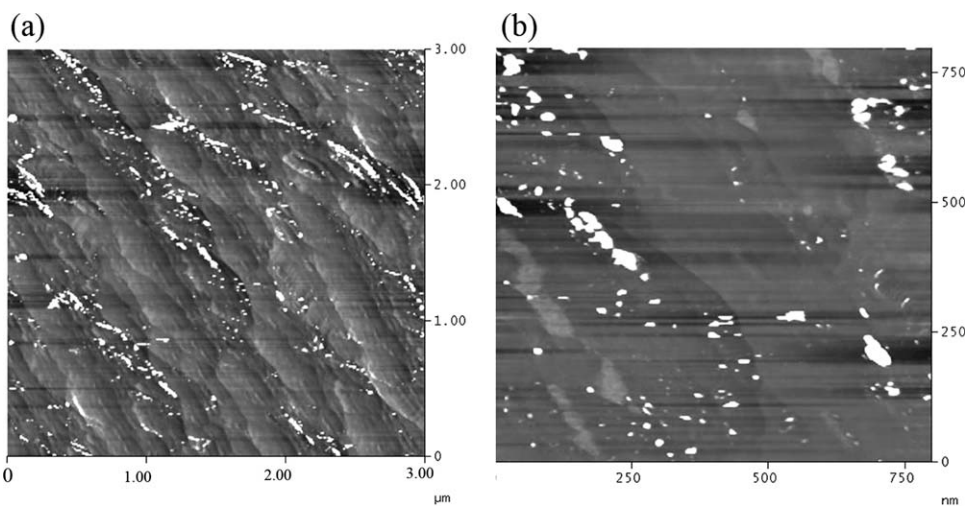

Figure 3 AFM phase images of NMSN30 at different magnifications.

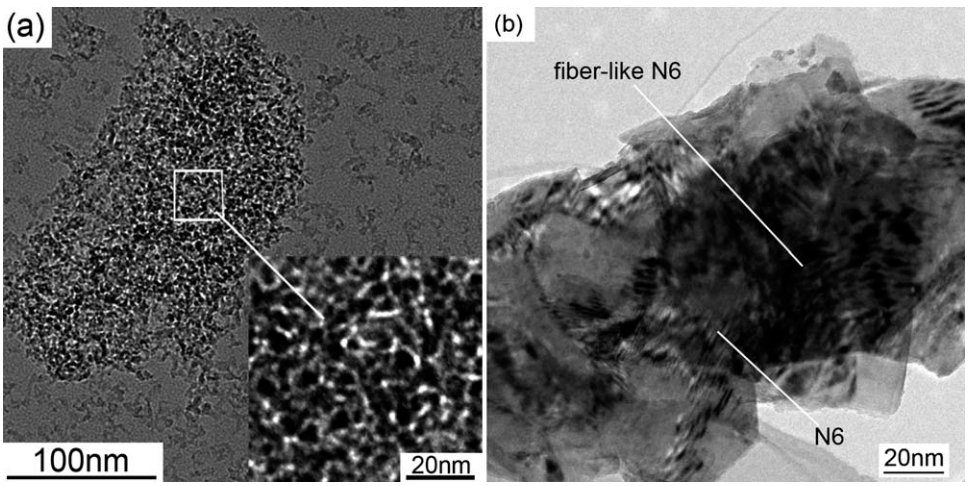

Figure 4 (a) TEM micrograph of MS obtained by sintering NMSN30 at 700°C for 8 h. (b) TEM micrograph of MS after N6 enwrapping the surface was washed away.

and the density of N6, it can be easily estimated that, in NMSN30 system, about 13.5 wt % of N6 is trapped in these mesopores. Certainly, the presence of a large amount of N6 in the mesopores of MS will lower the image contrast of silica particles obviously, which explains the reason why the MS particles look very vague when observed by TEM and why a clear image cannot obtained. It is reasonable to deduce that, at the same loading of silica, MS may have greater effects on the mechanical properties and crystallization behavior of N6 than PS.

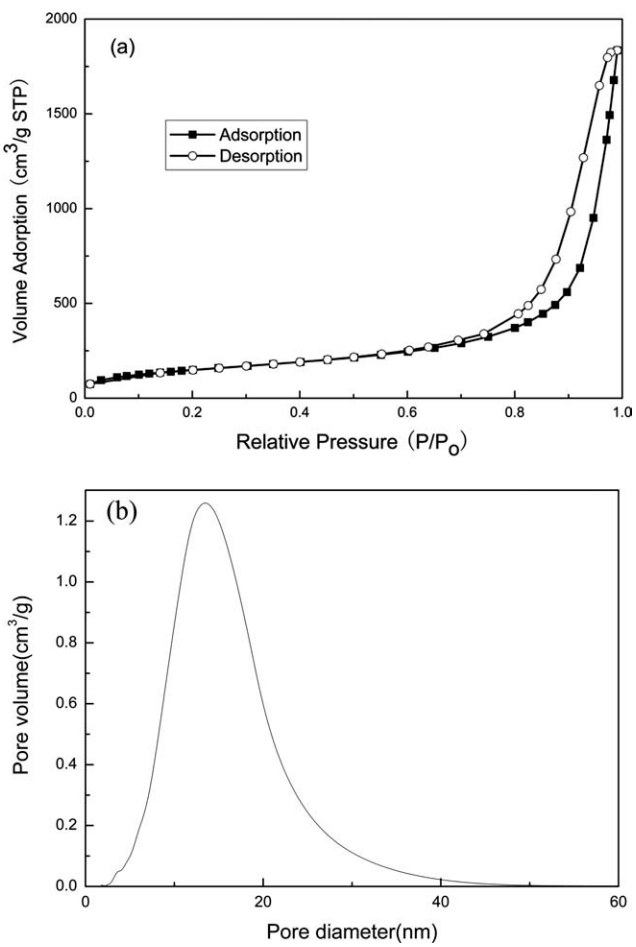

Figure 5 BET test curves of MS obtained by heating NMSN30 at 700°C for 8 h. (a) Nitrogen adsorption and desorption curve and (b) pore size distribution curve.

Although numerous polymer/silica nanocomposites have been successfully fabricated via sol–gel hybridization, this kind of MS filler generated *in situ* polymerization has never been reported. The key of our success lies in the fact that both silica network and N6 are generated synchronously. Because of the excellent compatibility of ε-caprolactam and silicic acid, at the initial stage of polymerization, the system is homogenous monophasic system. With the reaction proceeds, silica network forms and microphase separation occurs. However, due to the low loading of TEOS, it is impossible to form a silica network throughout the system. Instead, many nanosized silica networks form. During this process, some water, ε-caprolactam, and oligomer of N6 were enwrapped in these silica networks. Polymerization can still proceed in these swelling silica networks, and the N6 formed remains in the networks. The last stage of the polymerization was performed under high temperature and high vacuum. Under such a condition, the water enwrapped and

TABLE II
BET Surface Area, Total Pore Volume, and Average Pore Diameter of MS Generated *In Situ* and PS

Sample	BET surface area ($m^2\ g^{-1}$)	Single point adsorption total pore volume of pores ($cm^3\ g^{-1}$)	Adsorption average pore diameter (nm)
MS	632	3.21	14.2
PS	132	—	—

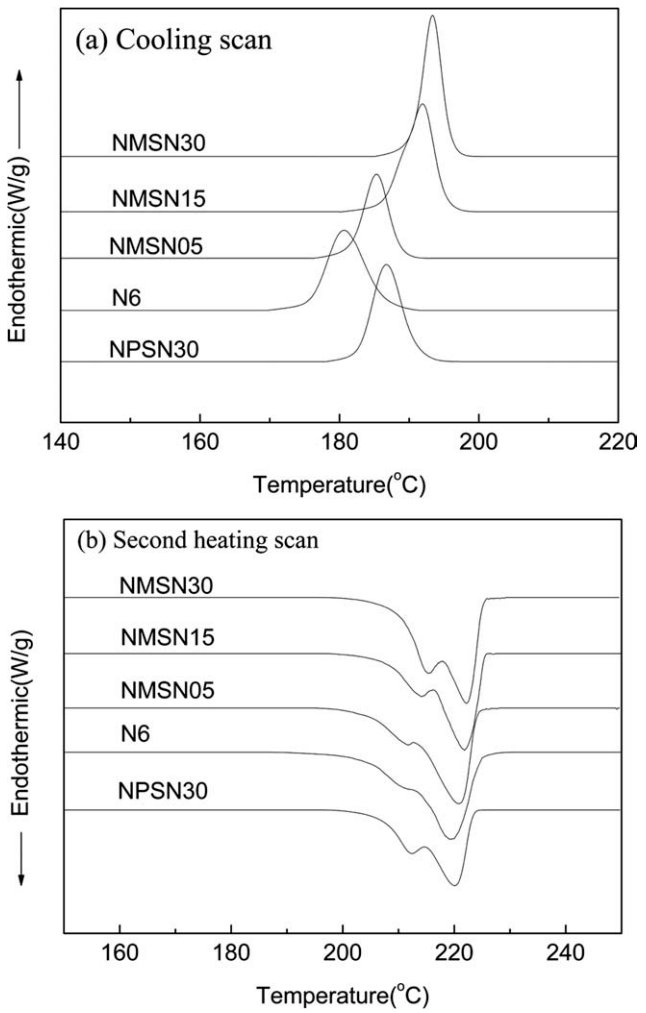

Figure 6 DSC curves of neat N6, NPSN30, and NMSNs. (a) cooling scan and (b) second heating scan.

generated by polycondensation, and unreacted ε-caprolactam monomer may serve as foaming agents. The quick release of these small molecules from the incompletely crosslinked silica network leads to the formation of many pores, and these formed pores will be occupied by N6 quickly. At last, when a fully crosslinked silica network forms, the porous structure is fixed. It should be noted that the mechanism proposed here is based purely on assumption, and the exact mechanism requires further investigation.

Crystallization behavior

The crystallization and melting behavior of N6, NPSN30, and NMSNs have been studied by DSC. The cooling curves and second heating curves are shown in Figure 6, and the data are summarized in Table III. It is seen from Figure 6(a) that the incorporation of MS leads to a considerable increase in crystallization temperature (T_c). In particular, the T_c of NMSN30 is 193.3°C, which is 12.7°C higher than that of N6 (180.6°C) and also 6.4°C higher than that of NPSN30 (186.9°C).

In Figure 6(b), N6 and its nanocomposites all show two melting peaks at about 213 and 220°C, ascribed to the melting peaks of the γ-crystalline form and α-crystalline form, respectively.[27,28] The lower temperature melting peak is designated as T_{m1}, while the higher temperature as T_{m2} in Table III. The melting peaks of γ-phase become obvious with the increasing loading of MS, indicating that the incorporation of MS favors the formation of the γ-crystalline form. The similar phenomenon has been observed in polyamide 6/clay nanocomposites by many researchers[29,30] and has been ascribed to the interaction between clay layers and polymer chain. Vaia et al.[31] suggested that the interaction between clay layers and polymer chains results in conformation changes of chains, limiting the formation of hydrogen-bonded sheets of the α-phase and favoring the formation of γ-phase. This explanation is also applicable to NMSNs system. Considering the ultrahigh SSA, the immobilizing effect of mesopores on N6, and the hydrogen bonds between polar amide group of N6 and the hydroxyl groups of MS, the chain mobility of N6 is also constrained effectively in the NMSNs system.

With the increasing loading of MS, the two melting points, T_{m1} and T_{m2}, shift to high temperature as shown in Table III. The T_{m2} of NMSN30 is 222.1°C, 2.9°C higher than that of neat N6, and also 1.8°C higher than NPSN30, indicating that the incorporation of MS may lead to the formation of more perfect crystals. As shown in Table III, it is surprising to find that the crystallinity ($X_{c(DSC)}$) is not obviously changed with increasing MS content. Although MS can promote crystallization by acting as nucleating agent, MS can also hinter the chain mobility of N6, as previously mentioned. Because of the coexistence of these two oppositing effects of MS on the crystallization behavior, the total crystallinity may change a little depending on the loading of MS.

TABLE III
Characteristic Values of Crystallization and Melting Behavior of N6, NPSN30, and NMSNs

	Cooling scan			Second heating scan	
Sample code	T_c (°C)	T_{m1} (°C)	T_{m2} (°C)	ΔH_f of N6 J g^{-1}	$X_{c(DSC)}$ (%)
N6	180.6	212.0	219.2	51.68	27.2
NMSN05	185.2	212.2	220.8	54.34	28.6
NMSN15	191.9	213.8	221.0	53.39	28.1
NMSN30	193.3	215.1	222.1	49.97	26.3
NPSN30	186.9	212.4	220.3	53.3	28.0

TABLE IV
Mechanical Properties and HDT of N6, NPSN30, and NMSNs

Samples codes	IZOD notched impact strength (J/m)	Flexural strength (MPa)	Flexural modulus (GPa)	Tensile strength (MPa)	Tensile modulus (GPa)	HDT, 1.82 MPa (°C)
N6	79.4	98.2	1.76	66.4	1.26	57.5
NMSN05	85.7	119.3	2.49	76	1.59	80.7
NMSN15	82.0	127.1	2.74	78.2	1.82	103.2
NMSN30	76.2	133.4	2.98	84.5	2.24	113.4
NPSN30	53.2	110	2.33	76.5	1.80	90.0

Mechanical properties

The mechanical properties and heat deflection temperature (HDT) of N6, NPSN30, and NMSNs are listed in Table IV. The incorporation of MS leads to a considerable improvement in mechanical properties, as shown in Table IV. In particular, the flexural modulus, flexural strength, tensile strength, and tensile modulus of NMSN30 increase by 69.3%, 35.8%, 27.3%, and 77.8%, respectively, compared to those of pure N6, and are also 27.9%, 21.3%, 13.3%, and 24.4% higher than those of NPSN30. It is obvious that, at the same loading of silica, MS has better reinforcement effect on N6 than PS.

The HDT of a polymeric material is an index of its heat resistance toward applied load. The incorporation of MS remarkably increases the HDT of N6. The HDT of NMSN30 is 113.4°C, which is 55.9°C higher than that of N6 (HDT = 57.5°C), and also 23.4°C higher than NPSN30 (HDT = 90.0°C). The increased HDT can be mainly ascribed to the constrained chain mobility. As mentioned, the HDT reflects the ability of a polymeric material to withstand loads at elevated temperature, and this is also a modulus-temperature behavior as elucidated by DMA.

The variation of storage modulus and loss factor of neat N6 and NMSN30 with temperature is shown in Figure 7. The incorporation of MS leads to a shift of the temperature of the main α-relaxation (T_α) toward high temperature, indicating that the mobility of N6 chain segments is obviously inhibited. This result is inconsistent with that of the polyamide 6,6/silica system prepared by sol–gel method,[20] in which the incorporation of silica decreases T_α obviously. This leads to the question as to what causes so great difference for these two systems. In polyamide 66/silica system, the silica is generated under low temperature; therefore, the conversion of TEOS and the crosslinking degree of silica is low, which leads to a comparatively high content of low molecules in the resulting composite. The plasticizing effect of these low molecules is responsible for the decreased T_α. However, in our study, the MS is generated under high temperature (250°C) and high vacuum (200–300 Pa) for long time; therefore, a fully crosslinked silica network and full conversion of TEOS are guaranteed. It is known that the peak height of the loss tangent curve indicates the chain flexibility of the polymer chains that undergo resonance with the externally applied sinusoidal stress. The more flexible the chains are, the higher the amplitude of vibration would be.[16,32] It is seen from Figure 7 that the tan δ_{max} of NMSN30 is much lower than that of N6, which indicates that strong interface interaction exists between N6 and MS.

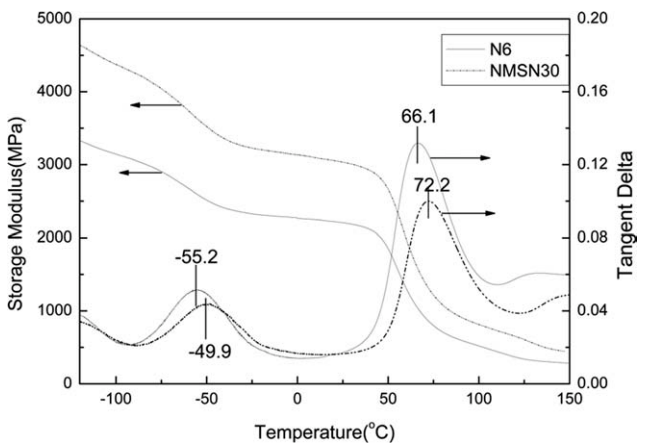

Figure 7 Storage modulus and loss factor of neat N6 and NMSN30.

The β-relaxation is related to the movement of the polar groups of N6. The temperature of the β-relaxation (T_β) of NMS30 is observed at −49.9°C, 5.3°C higher than that of N6 (−55.2°C), which indicates that the movement of polar groups of N6 is also constrained by the incorporation of MS.

From Figure 7, it is seen that the storage modulus increases with the addition of MS. The improvement in the storage modulus of the NMSN30 is mainly due to the stiff nature of the MS and the combined effect of the ultrahigh SSA and fine dispersion of MS. In addition, the strong interface interaction and the immobilizing effect of MS on N6 play positive role on the improvement of the storage modulus.

CONCLUSIONS

In situ synchronous growth of silica and N6 leads to the formation of mesoporous structure of MS.

Compared to conventional PS, MS shows better ability in improving mechanical properties and increasing HDT, which can be ascribed to the ultrahigh SSA, strong interface interaction, and the immobilizing effect of mesopores on N6. In particular, at a loading of 3 wt % MS, the flexural modulus, flexural strength, tensile modulus, and HDT of NMSN exhibit increase of about 69.3%, 35.8%, 77.8%, and 55.9°C, respectively. DSC results show that the incorporation of MS influences the crystallization behaviors of N6 obviously: (1) increases T_c by serving as heterogonous nucleating agent, leading to the formation of more perfect crystals; (2) favors the formation of γ-phase by hindering the mobility of N6 chains. DMA analysis shows that compared to that of neat N6, the temperature of the main α-relaxation (T_α) and secondary β-relaxation (T_β) is shifted 6.1°C and 5.3°C toward higher temperature, respectively, indicating that the chain mobility of N6 is effectively constrained by the incorporation of MS.

References

1. Sadhu, S.; Bhowmick, A. K. J Polym Sci 2004, 42, 1573.
2. Tarapow, J. A.; Bernal, C. R.; Alvarez, V. A. J Appl Polym Sci 2009, 111, 768.
3. Hambir, S.; Bulakh, N.; Kodgire, P.; Kalgaonkar, R.; Jog, J. P. J Polym Sci 2001, 39, 446.
4. Huang, Z. H.; Qiu, K. Y. Polymer 1997, 38, 521.
5. Mo, T. C.; Wang, H. W.; Chen, S. Y.; Dong, R. X.; Kuo, C. H.; Yeh, Y. C. J Appl Polym Sci 2007, 104, 882.
6. Armelao, L.; Barreca, D.; Bottaro, G.; Gasparotto, A.; Tondello, E.; Ferroni, M.; Polizzi, S. Chem Mater 2004, 16, 3331.
7. Schottner, G. Chem Mater 2001, 13, 3422.
8. Fitzgerald, J. J.; Landry, C. J.; Pochan, J. M. Macromolecules 1992, 25, 3715.
9. Landry, C. J.; Coltrain, B. K.; Landry, M. R.; Fitzgerald, J. J.; Long, V. K. Macromolecules 1993, 26, 3702.
10. Yeh, J. M.; Huang, K. Y.; Dai, C. F.; Chand, B. G.; Weng, C. J. J Appl Polym Sci 2008, 110, 2108.
11. Tangpasuthadol, V.; Intasiri, A.; Nuntivanich, D.; Niyompanich, N.; Kiatkamjornwong, S. J Appl Polym Sci 2008, 109, 424.
12. Suzuki, F.; Onozato, K.; Kurokawa, Y. J Appl Polym Sci 1990, 39, 371.
13. Araki, W.; Adachi, T. J Appl Polym Sci 2008, 107, 253.
14. Wen, J. Y.; Mark, J. E. J Appl Polym Sci 1995, 58, 1135.
15. Bandyopadhyay, A.; Mousumi, D. S. J Appl Polym Sci 2004, 93, 2579.
16. Bandyopadhyay, A.; Sarkar, M. D.; Bhowmick, A. K. J Appl Polym Sci 2005, 95, 1418.
17. Wang, S. H.; Ahmad, Z.; Mark, J. E. Chem Mater 1994, 6, 943.
18. Kioul, A.; Mascia, L. J Non-Cryst Solids 1994, 175, 169.
19. Qin, J. Q.; Zhao, H.; Liu, X. Y.; Zhang, X. Y.; Gu, Y. Polymer 2007, 48, 3379.
20. Sengupta, R.; Bandyopadhyay, A.; Sabharwal, S.; Chaki, T. K.; Bhowmick, A. K. Polymer 2005, 46, 3343.
21. Zhao, C. G.; Hu, G. J.; Justice, R.; Schaefer, D. W.; Zhang, S. M.; Yang, M. S. Polymer 2005, 46, 5125.
22. Liu, A. D.; Xie, T. X.; Yang, G. S. Macromol Rapid Comm 2006, 27, 1572.
23. Ou, Y. C.; Yang, F.; Yu, Z. Z. J Polym Sci 1998, 36, 789.
24. Wu, Q.; Liu, X. H.; Berglund, L. A. Macromol Rapid Commun 2001, 22, 1438.
25. Campoy, I.; Gomez, M. A.; Marco, C. Polymer 1998, 39, 6279.
26. Davis, M. E. Nature 2002, 417, 813.
27. Pierron, L. P.; Depecker, C.; Seguela, R.; Lefebvre, J. M. J Polym Sci 2001, 39, 484.
28. Khanna, Y. P.; Kuhn, W. P. J Polym Sci 1997, 35, 2219.
29. Liu, X. H.; Wu, Q. J.; Berglund, L. A. Polymer 2002, 43, 4967.
30. Mathias, L. J.; Davis, R. D.; Jarrett, W. L. Macromolecules 1999, 32, 7958.
31. Lincoln, R. M.; Vaia, R. A.; Wang, Z. G.; Hsiao, B. S. Polymer 2001, 42, 1621.
32. Thavamani, P.; Bhowmick, A. K. J Mater Sci 1992, 27, 3243.